

WFPC2 Observations of Massive and Compact Young Star Clusters in M31¹

Benjamin F. Williams
 University of Washington
 Astronomy Dept. Box 351580, Seattle, WA 98195-1580
 ben@astro.washington.edu

Paul W. Hodge
 University of Washington
 Astronomy Dept. Box 351580, Seattle, WA 98195-1580
 hodge@astro.washington.edu

ABSTRACT

We present color magnitude diagrams of four blue massive and compact star clusters in M31: G38, G44, G94, and G293. The diagrams of the four clusters reveal a well-populated upper main sequence and various numbers of supergiants. The U-B and B-V colors of the upper main sequence stars are used to determine reddening estimates of the different lines of sight in the M31 disk. Reddening values range from $E_{B-V} = 0.20 \pm 0.10$ to 0.31 ± 0.11 . We statistically remove field stars on the basis of completeness, magnitude and color. Isochrone fits to the field-subtracted, reddening-corrected diagrams yield age estimates ranging from 63 ± 15 Myr to 160 ± 60 Myr. Implications for the recent evolution of the disk near NGC 206 are discussed.

Subject headings: galaxies: M31; spiral; stellar populations; star clusters.

1. Introduction

Studies of the stellar content of extra-galactic globular clusters (hereafter GCs) started in the Magellanic Clouds (e.g. Shapley 1930). These observations led to the recognition of several blue GCs whose ages were found to range from $\sim 10^8$ - 10^9 years (Arp 1958; Arp 1959; Hodge 1961; Hodge & Schommer 1984; Brocato et al. 1989; and many others). The Galaxy appears not to have such young massive and compact clusters, though other more distant spirals do (Larsen & Richtler 1999). If they are young GCs, observations may uncover valuable clues about the formation and evolution of GCs. Regardless of their classification, these clusters are certainly useful probes of the reddening in their portion of the galaxy because they contain upper main sequence stars at a common distance, which have nearly the same color in B-V independent of metallicity.

Using photoelectric photometry, van den Bergh (1969) observed that some of the objects in M31 classified as GCs were very blue, including the four clusters discussed here: G38, G44, G94, and G293 (designations are from Sargent et al. 1977). Integrated U, B, and V photometry of hundreds of clusters was done with photographic plates by Battistini et al. (1987), confirming the blue colors of these four and several others. With the Ultraviolet Imaging Telescope aboard the Astro-1 mission, Bohlin et al. (1993)

¹Based on observations with the NASA/ESA Hubble Space Telescope obtained at the Space Telescope Science Institute, which is operated by the Association of Universities for Research in Astronomy, Inc., under NASA contract NAS5-26555.

detected 43 M31 GCs in the ultraviolet, including G94, and its UV flux was consistent with its being a young cluster. Huchra, Kent, & Brodie (1991) completed spectroscopic metallicity measurements for 150 GCs in M31, including G38. Its metallicity measurement has high uncertainty and may be significantly underestimated because it was determined without the knowledge of its young age.

The first M31 globular cluster resolved into stars was studied from the ground by Heasley et al. (1988). With sub-arcsecond seeing observations from Mauna Kea, they resolved the red giant branch of G1. More recently, the populations of star clusters in M31 have been resolved with from space (e.g. Ajhar et al. 1996, Rich et al. 1996, Pecci et al. 1996, Holland, Fahlman, & Richer 1997, Jablonka et al. 2000). These studies have used images from the Wide Field and Planetary Camera (WFPC-2) aboard the Hubble Space Telescope (HST) to construct color-magnitude diagrams (CMDs) of M31 star clusters in order to determine their metallicities, reddening values, and ages; in some cases, comparisons were made between the cluster and field populations (e.g. Jablonka et al. 2000). We are using the same instrument to make CMDs of four of the massive and compact young clusters: G38, G44, G94 and G293.

We begin in section 2 with a description of our observations and reduction techniques, followed in section 3 by the details of our field subtraction technique. In section 4 we discuss the determination of the reddening values and luminosity determinations for each cluster, and section 5 describes the age determinations. Finally, in section 6 we provide a summary of our results.

2. Observations and Data Reduction

All observations for this project were obtained through the F336w, F439w, and F555w filters with the WFPC-2 imager aboard HST on October 15,16,30, and 31, 1999. Each field had 3600 seconds of exposure in F336w, 1600 seconds in F439w, and 1200 seconds in F555w. The short exposure times were ideal for controlling field contamination by disk stars of M31, minimizing the severe crowding expected in these dense clusters, and minimizing telescope time needed.

The images were well aligned so that no shifting was necessary before combining. They were combined using the IRAF task gcombine, with the cosmic ray rejection algorithm crreject, and the photometry was extracted using the automated photometry programs DAOPHOT-II and ALLSTAR (Stetson, Davis, & Crabtree 1990). DAOPHOT-II finds the stars in the image and generates a point spread function (PSF) from the stars which are both isolated enough to minimize neighbors contaminating the PSF measurement and bright enough to provide high signal to noise for the PSF measurement. Allstar groups the stars together and carries out the photometry in such a way as to not include counts from neighboring stars when fitting the PSF. With these programs, it is possible to obtain fairly accurate photometry for crowded fields. PSF magnitudes were checked against aperture photometry of the most isolated stars with the highest signal to noise in order to determine if there was an offset between the PSF photometry and the more standard aperture photometry; results are shown in Figure 1. Within the errors of our photometry there was no significant aperture correction. Due to the shallowness of our images, and the fluctuation of the background level in the structured disk of M31, the accuracy of our photometry was not high. As shown in Figure 2, the photometric accuracy was worse for the bluer observations; the average errors were 0.16 mag in U, 0.13 mag in B, and 0.10 mag in V. From the data shown in Figure 1, we calculate internal uncertainties of 0.06 mag for the F336W data, 0.10 mag for the F439W data, and 0.02 mag for the F555W data for the best sampled, most isolated cases (rms).

We obtained standard U, B, and V magnitudes from our photometry using the methods, zero

points, and transformation coefficients given in Holtzman et al. (1995). We first determined instrumental magnitudes for the F336w, F439w, and F555w filter as

$$m_{filter} = -2.5 \times \log(ADU/t) + ZP_{filter} \quad (1)$$

where ADU is the number of counts, t is the exposure time, and ZP_{filter} is the zero point of the WFPC-2 chip for the bandpass. Since the transformation to U, B, and V is a function of color, we used the F336w - F439w as a first approximation of the U-B color and the F439w - F555w color as a first approximation of the B-V color and iteratively solved the transformation equations.

3. Field Contamination

To make sure that we sampled the whole cluster, we made CMDs containing all the stars within 11.5" of the cluster center (43 pc). We chose this radius because it was about twice the radius where the difference between the star density and the average star density of the field became comparable to the fluctuations of the field star density. These CMDs are shown for each cluster in Figure 3. They show a conspicuous main sequence with a few scattered red stars. In order to remove field stars from our cluster CMD, we determined the completeness of our data as a function of color and magnitude, inside and outside the cluster. With quantitative knowledge of the completeness, we could calculate how many field stars our photometry measured inside the cluster.

3.1. Completeness Tests

In order to do accurate field subtraction in the cluster region, we determined how well our photometry routine detected stars in different regions of the chip for each cluster. We expected the completeness to be worse at fainter magnitudes and closer to the cluster center, but it was necessary to quantify this effect in order to determine the correct number of field stars at each color and magnitude that were detected inside the cluster.

We added a unique list of 500 artificial stars to each of 20 copies of each cluster image, making a total of 10000 artificial test stars for each cluster. Adding only 500 stars to each image copy insured that the crowding of the artificial stars themselves would not effect the completeness results. We put each image copy through the same photometry routine that we used for our original data in order to learn the completeness and accuracy with which the artificial stars were recovered. We ran more tests closer to the center of the cluster, and more at fainter magnitudes to improve our sampling where we thought the completeness would be the worst.

Examples of the results of our artificial star tests are shown in Figure 4. Dotted contours show where the completeness was less than ten percent (0.5 and 5 percent). The first solid contour marks ten percent completeness, and successive contours each mark five percent increases in completeness, so that the thick contours mark 25, 50, and 75 percent completeness. Above 80 percent is not as systematic because of the small number of stars at bright magnitudes far away from the cluster. We found that in general our photometry was greater than 10% complete down to $m_B \approx 25$, but completeness decreased substantially inside of one arcsecond from the cluster center, as expected. The effect was quite different for the four clusters supporting the impression that the clusters are not equally compact; G38 and G44 are much more crowded in their central arcsecond than G94 or G293.

3.2. Field Subtraction

We used the color information of our completeness tests as well as position and brightness information to determine the field contamination in our cluster CMDs. We accomplished this multi-dimensional analysis by making different CMDs of the artificial stars for 3 different annuli around the cluster center. We divided each of our artificial CMDs for the three annuli into bins of color and magnitude. By examining the artificial stars in each bin, we calculated the completeness for each magnitude and color in each annulus.

Using the CMDs of the field stars for each cluster (Figure 5), we measured the number of field stars in each color and magnitude bin. After correcting these measurements for the completeness inside the cluster, we removed the proper number of stars from each color magnitude bin in the cluster CMD. The final field subtracted and reddening corrected CMDs for all four clusters are given in Figure 6. (The reddening correction will be discussed in the next section.) Notice that the fainter red stars, along with a reasonable fraction of the main sequence stars, have disappeared. Also interesting is the varying number of supergiants from cluster to cluster. For example G38 and G94 appear to have significantly more supergiants than G44 or G293.

4. Determination of Reddening and Integrated Cluster Parameters

In order to determine the reddening, we assumed that the reddening law of M31 is the same as the reddening law in our Galaxy. This assumption has been true for most observations of reddening in M31 (e.g. Waltherbos & Kennicutt 1988; Nedialkov & Ivanov 1999; Barmby et al. 2000). We therefore assumed that $E_{U-B} = 0.64E_{B-V}$ (Binney & Merrifield 1998), and we used the colors from the model main sequence of Bertelli et al. (1994) in order to determine the reddening of our cluster stars.

One advantage of looking at blue clusters is that they often contain upper main sequence stars, which have B-V colors that are nearly independent of absolute magnitude. These stars are easily corrected to their intrinsic colors in the B-V, U-B plane. All of our clusters contained a significant number of these stars. We used all the stars blueward of B-V = 0.5, and brighter than $m_V = 24.5$ in order to determine our reddening correction. With the random errors in our photometry, however, they did not make a typical linear sequence in the B-V, U-B plane. Instead, they were spread in a Gaussian-like way to the red of the main sequence line.

We determined the average and standard errors of this distribution of stars, under the assumption that all of their true B-V colors were nearly equal. Using these values, we assumed an error ellipse whose axes corresponded to the standard deviation of the B-V and U-B colors. We then shifted the error ellipse along the reddening line until ten percent of the area crossed the theoretical main-sequence color line, and again until 90 percent of the area crossed the line. We took these limits to be the lower and upper limits of the reddening correction at the 90 percent confidence level, and we took the shift which centered the distribution on the model main sequence to be the most likely value predicted by our data. This most likely shift for each cluster is shown in Figure 7. Solid lines show the model colors for stars on the main sequence (top curve), and supergiants (bottom curve). The dotted line shows the reddening line. Closed boxes are average colors of the pre-corrected upper main sequence stars, and open boxes are the same distributions after applying our most likely reddening correction value. Three of our clusters had reddening values close to the mean value of globulars in M31 determined by Barmby et al. (2000) from a sample of 221 clusters to be $E_{B-V} = 0.22$. The larger value for G38 is reasonable since the lower number of field stars near that cluster may be due to a higher extinction level.

We obtained the half-light radii and the integrated fluxes of the clusters by measuring the average flux per pixel in the field, *including* the field stars. We then subtracted off this background and measured the total flux coming from the cluster for different aperture sizes. At the same time, we measured the surface brightness at each radius, in order to determine the radius at which the difference between the surface brightness and the average surface brightness of the field was the same as the fluctuations in the surface brightness of the field. We took our measurement of the total flux inside an aperture of this radius. We then measured the half-light radius, the aperture size where the flux was 1/2 this total value.

In Table 1 we give:

Column 1: The name of each cluster from Sargent et al. (1977).

Column 2: Our values for the projected galactocentric distances in kpc.

Column 3: Our measured half-light radii, typical errors were ± 0.3 pc.

Columns 4, 5, 6: Integrated U, B, and V magnitudes from Battistini et al. (1987). Their typical errors were ± 0.15 .

Column 7: Our values for the reddening (E_{B-V}) determined using U, B, and V stellar photometry.

Columns 8, 9, 10: The reddening corrected U, B, and V integrated magnitudes from our data. Typical errors were ± 0.10 .

Column 11: The absolute V magnitude assuming a distance modulus of 24.43 (Freedman & Madore 1990). For comparison, a typical M_V for a globular cluster in our Galaxy is -7.1.

5. Ages

We determined ages by two different methods. First, we used the automated software package MATCH (Dolphin 1997). This software uses the artificial star results, uncertainties from the artificial star results, the photometry of the cluster stars, and the distance to the cluster to create color magnitude matrices (Hess diagrams). It then compares these Hess diagrams to scaled theoretical Hess diagrams, based on Bertelli isochrones (Bertelli et al. 1994), producing a modified χ^2 value for a given range of age, metallicity, and reddening values. Then it compares the quality of all of the fits to determine the most likely age, metallicity, and reddening values and an associated error for each. The program only works with two colors, B and V, so that the reddening values it derives may not be as reliable as those we determined using three colors.

As an independent age determination, using the stellar evolution models of Bertelli et al. (1994), we created isochrones for different ages and metallicities. We then looked at the different isochrones overplotted on our CMDs in order to determine a reasonable upper and lower limit on the age. The method is shown in Figure 8, where dotted lines mark the upper and lower limits. These were determined by finding the age where the blue loops fell below and above the location of the supergiants. The solid isochrones mark our choices for the best fits for the turnoff age. While the turnoff age was unaffected by the chemical composition at these young ages, the distribution of supergiants was often more consistent with one metallicity than another. While we make no claims here to have robust measurements of the metallicities for these clusters, we label the metallicities here in order to be complete in our descriptions of the best fitting isochrones.

The results for both techniques are shown in Table 2, which gives the ages, metallicities and errors determined by eye using isochrone fitting, and the ages, metallicities and errors determined by MATCH,

using statistical comparisons of Hess diagrams. Clearly, the two methods derived consistent ages and metallicities, but the quoted errors from the isochrone fitting are smaller. This is likely due to the fact that we estimated the isochrone errors assuming that our reddening value is correct, whereas the uncertainties in the reddening measurements were folded into the errors that MATCH derived.

Magnier et al. (1997) studied the young stellar population and Cepheid variable population of this region of the M31 disk in detail. They found that the average stellar ages in the region south of NGC 206 (~ 90 Myr) are slightly older than NCG 206 (~ 30 Myr) but younger than the population to the north of NGC 206, suggesting that the density wave interaction that is coincident with the location of NGC 206 has been propagating through the galaxy at ~ 32 km/s. G38 and G44 are located near the center of the overdensity of Cepheids that they find to the south of NGC 206. Our ages for these massive clusters show that they were likely formed at the same time as the Cepheids in the surrounding region. Assuming a distance modulus to M31 of 24.43 (Freedman & Madore 1990), these clusters are located at projected distances ~ 3500 pc and ~ 2600 pc south-southwest of NGC 206, respectively. Therefore, these ages for G38 and G44 strengthen the argument that the spiral arm interaction possibly responsible for the creation of NCG 206 has been propagating through M31 from south to north at a projected speed of ~ 32 km/s with respect to the stars in the disk. In fact, these ages are consistent with the possibility that these clusters were formed by the same mechanism that has caused the formation of NGC 206.

6. Conclusions

We have constructed CMDs for four massive and compact star clusters in the disk of M31. The CMDs reveal an upper main sequence stellar population showing that these are indeed young clusters. The reddening values determined using the color of the upper main sequence stars are comparable to typical reddening values determined for globular clusters in the M31 halo, suggesting that three of these clusters may be closer to the near side of the disk. The fourth case shows higher reddening, suggesting that it is located deeper in the disk. None of the reddening values are extremely high, which suggests that these clusters have formed in regions of relatively low dust content.

Age determinations from statistical matching of CMD properties as well as those from isochrone fitting give consistent ages for all four clusters. These ages range from 63 ± 15 Myr to 160 ± 60 Myr. The ages of G38 and G44 show that they formed at the same time as the well-studied surrounding Cepheid population, strengthening the conclusions of Magnier et al. (1997). The clusters' luminosities and half light radii imply that they are more massive and compact than any young clusters in our Galaxy; however, their luminosities are quite similar to young clusters found in many other galaxies (Larsen & Richtler 1999). Apparently, these massive and compact young clusters are common to most galaxies, including the Magellanic Clouds and M31, and it is very curious that our Galaxy contains no similar clusters.

7. Acknowledgments

We thank Ted Wyder for his help with the analysis methods; Andrew Dolphin for helping with the MATCH package; Andrew Becker for helping with the reduction and analysis programming; and Frank van den Bosch for helping to create some of the plots. Support for this work was provided by NASA through grant number GO-06459.01-95A from the Space Telescope Science Institute, which is operated by the Association of Universities for Research in Astronomy, Incorporated, under NASA contract NAS5-26555.

REFERENCES

- Ajhar, E. A., Grillmair, C. J., Lauer, T. R., Baum, W. A., Faber, S. M., Holtzman, J. A., Lynds, C. R., & O’Neil, J., E. J. 1996, *AJ*, 111, 1110
- Arp, H. 1959, *AJ*, 64, 175
- Arp, H. C. 1958, *AJ*, 63, 273
- Barmby, P., Huchra, J. P., Brodie, J. P., Forbes, D. A., Schroder, L. L., & Grillmair, C. J. 2000, *AJ*, 119, 727
- Battistini, P., Bonoli, F., Braccisi, A., Federici, L., Fusi Pecci, F., Marano, B., & Borngen, F. 1987, *A&AS*, 67, 447
- Bertelli, G., Bressan, A., Chiosi, C., Fagotto, F., & Nasi, E. 1994, *A&AS*, 106, 275
- Binney, J., & Merrifield, M. 1998, "Galactic astronomy" (Galactic astronomy / James Binney and Michael Merrifield. Princeton, NJ : Princeton University Press, 1998. (Princeton series in astrophysics))
- Bohlin, R. C., et al. 1993, *ApJ*, 417, 127
- Brocato, E., Buonanno, R., Castellani, V., & Walker, A. R. 1989, *ApJS*, 71, 25
- Dolphin, A. 1997, *New Astronomy*, 2, 397
- Freedman, W. L., & Madore, B. F. 1990, *ApJ*, 365, 186
- Heasley, J. N., Friel, E. D., Christian, C. A., & Janes, K. A. 1988, *AJ*, 96, 1312
- Hodge, P. W. 1961, *ApJ*, 133, 413
- Hodge, P. W., & Schommer, R. A. 1984, *PASP*, 96, 28
- Holland, S., Fahlman, G. G., & Richer, H. B. 1997, *AJ*, 114, 1488
- Holtzman, J. A., Burrows, C. J., Casertano, S., Hester, J. J., Trauger, J. T., Watson, A. M., & Worthey, G. 1995, *PASP*, 107, 1065
- Huchra, J. P., Kent, S. M., & Brodie, J. P. 1991, *ApJ*, 370, 495
- Jablonka, P., Courbin, F., Meylan, G., Sarajedini, A., Bridges, T. J., & Magain, P. 2000, *A&A*, 359, 131
- Larsen, S. S., & Richtler, T. 1999, *A&A*, 345, 59
- Magnier, E. A., Prins, S., Augusteijn, T., van Paradijs, J., & Lewin, W. H. G. 1997, *A&A*, 326, 442
- Nedialkov, P. L., & Ivanov, V. D. 1999, *A&AT*, 17, 367
- Pecci, F. F., et al. 1996, *AJ*, 112, 1461
- Rich, R. M., Mighell, K. J., Freedman, W. L., & Neill, J. D. 1996, *AJ*, 111, 768
- Sargent, W. L. W., Kowal, C. T., Hartwick, F. D. A., & van den Bergh, S. 1977, *AJ*, 82, 947
- Shapley, H. 1930, *Harvard Obs. Monographs No. 2* (Harvard)

Stetson, P. B., Davis, L. E., & Crabtree, D. R. 1990, in ASP Conf. Ser. 8: CCDs in astronomy, 289

van den Bergh, S. 1969, ApJS, 19, 145

Walterbos, R., & Kennicutt, R. 1988, A&A, p. 61

Table 1. Global parameters of our four clusters; typical errors are given in the text. The subscript “c” indicates a reddening corrected magnitude.

Name	GCD	$r_{1/2}$ (pc)	$m_{U_{\text{bat}}}$	$m_{B_{\text{bat}}}$	$m_{V_{\text{bat}}}$	E_{B-V}	m_{U_c}	m_{B_c}	m_{V_c}	M_{V_c}
G38	14.1	3.7	16.63	16.50	16.28	0.31	14.99	15.36	15.27	-9.16
G44	13.2	3.5	17.81	17.90	17.71	0.23	16.34	16.67	16.71	-7.72
G94	10.0	5.3	18.16	18.17	17.78	0.20	16.98	17.41	17.36	-7.07
G293	10.4	2.9	17.93	18.39	18.18	0.20	16.95	17.49	17.45	-6.98

Table 2. Ages and metallicities determined by isochrone fitting (columns 2 and 4) and by statical comparison of theoretically derived CMD’s (columns 3 and 5).

Name	Age_{iso} (Myr)	$\text{Age}_{\text{match}}$ (Myr)	Z_{iso}	Z_{match}
G38	100 ± 40	99 ± 67	0.008 ± 0.01	0.014 ± 0.02
G44	100 ± 40	83 ± 68	0.008 ± 0.01	0.013 ± 0.02
G94	160 ± 60	136 ± 54	0.008 ± 0.01	0.016 ± 0.02
G293	63 ± 15	40 ± 40	0.02 ± 0.01	0.016 ± 0.02

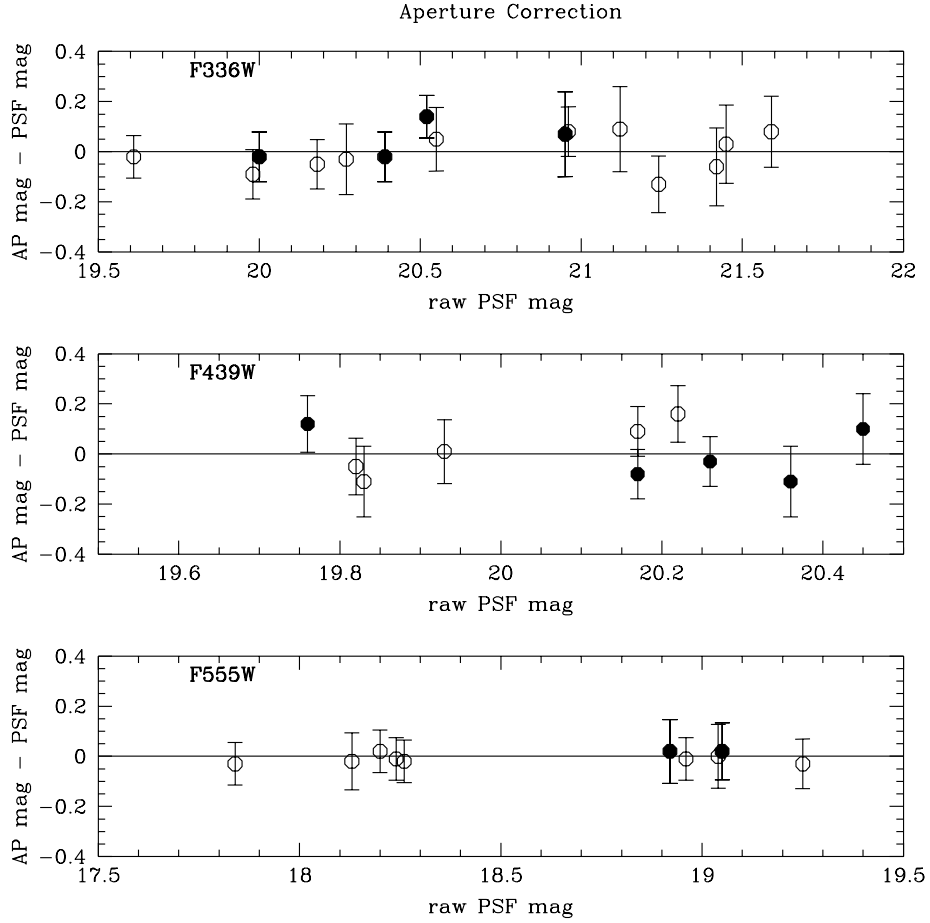


Fig. 1.— The residuals of the comparison of aperture magnitudes with the PSF magnitudes for the best sampled stars from the 3 bandpasses. Filled hexagons are isolated stars. Open hexagons have subtracted neighbors within the aperture.

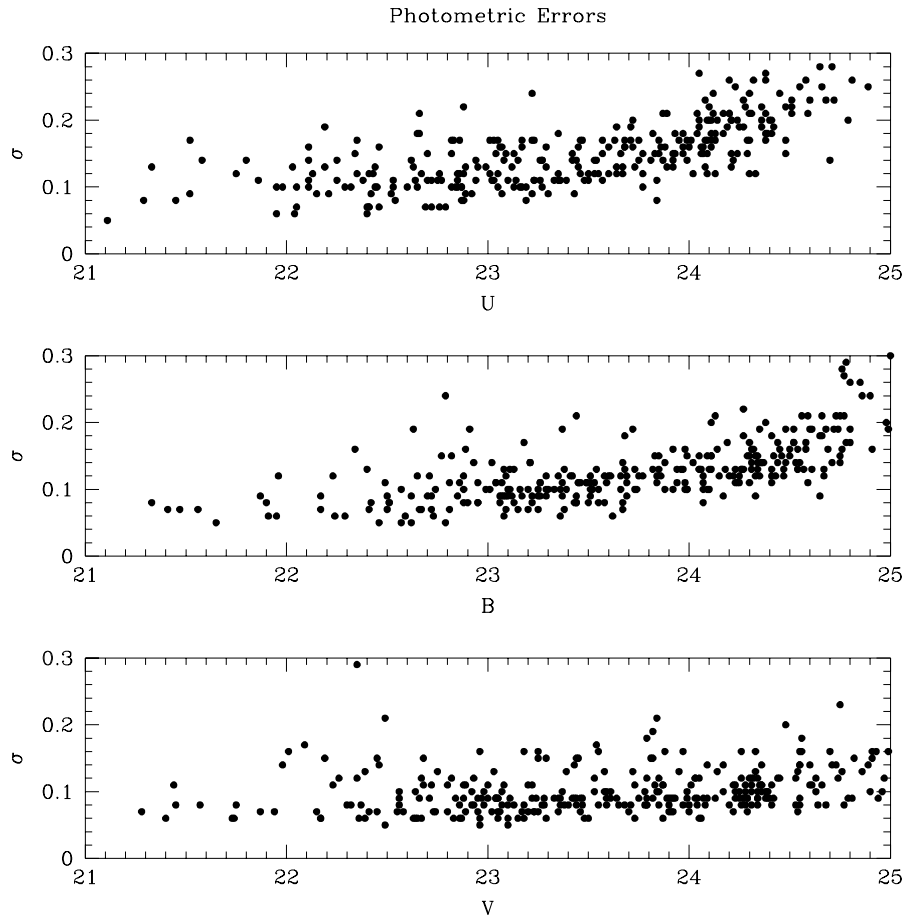


Fig. 2.— The calculated photometric errors for the stars in U, B, and V as a function of magnitude.

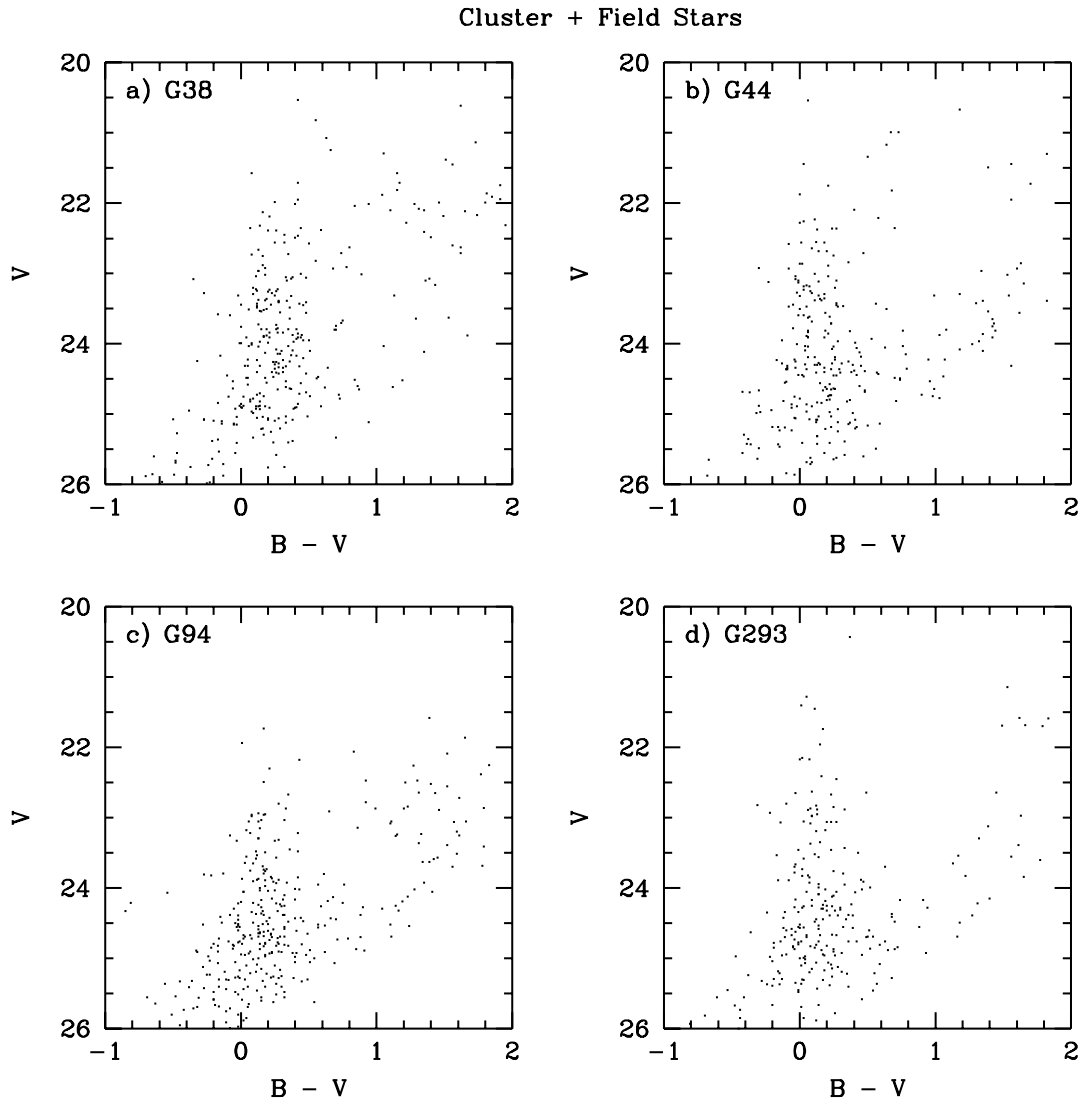


Fig. 3.— CMDs of the 4 clusters before field subtraction or reddening correction. The upper main sequence is apparent near $B - V = 0$. Field stars are peppered over the red side of the diagram.

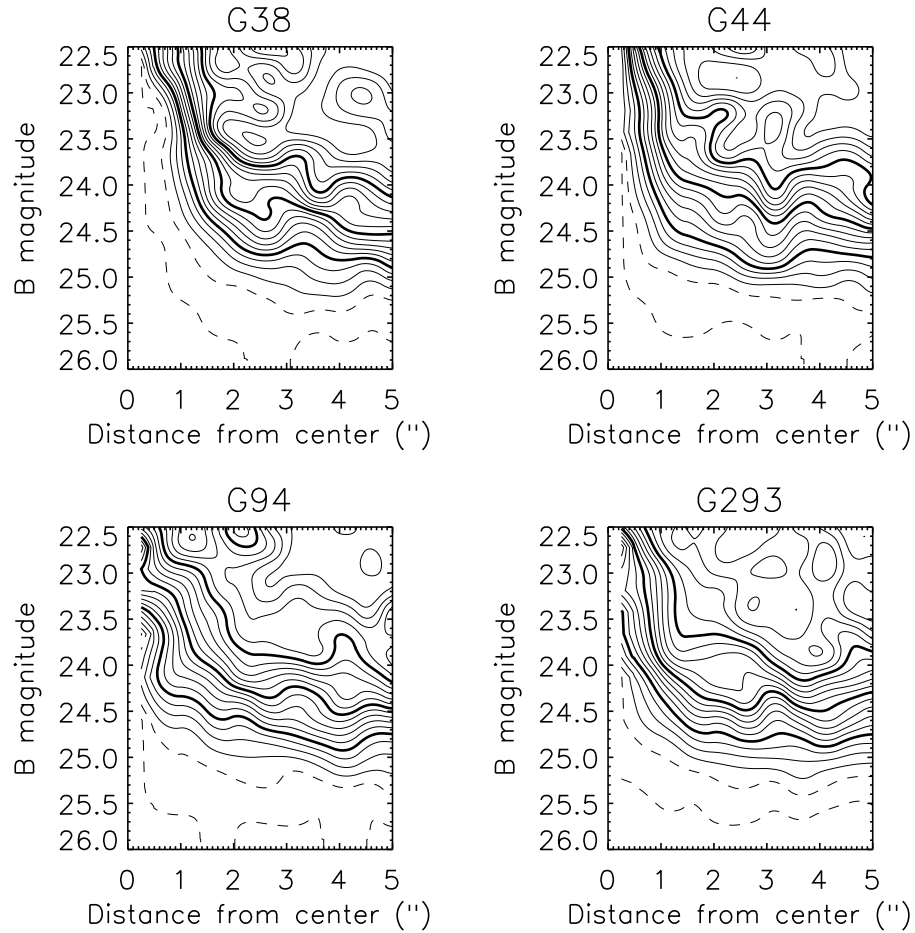


Fig. 4.— Completeness for the four clusters as a function of distance from the cluster center and apparent B magnitude. Dotted contours show where the completeness was less than ten percent (0.5 and 5 percent). The first solid contour marks ten percent completeness, and successive contours each mark five percent increases in completeness, so that the thick contours mark 25, 50, and 75 percent completeness. Above 80 percent is not as systematic due to less sampling at bright magnitudes far away from the cluster.

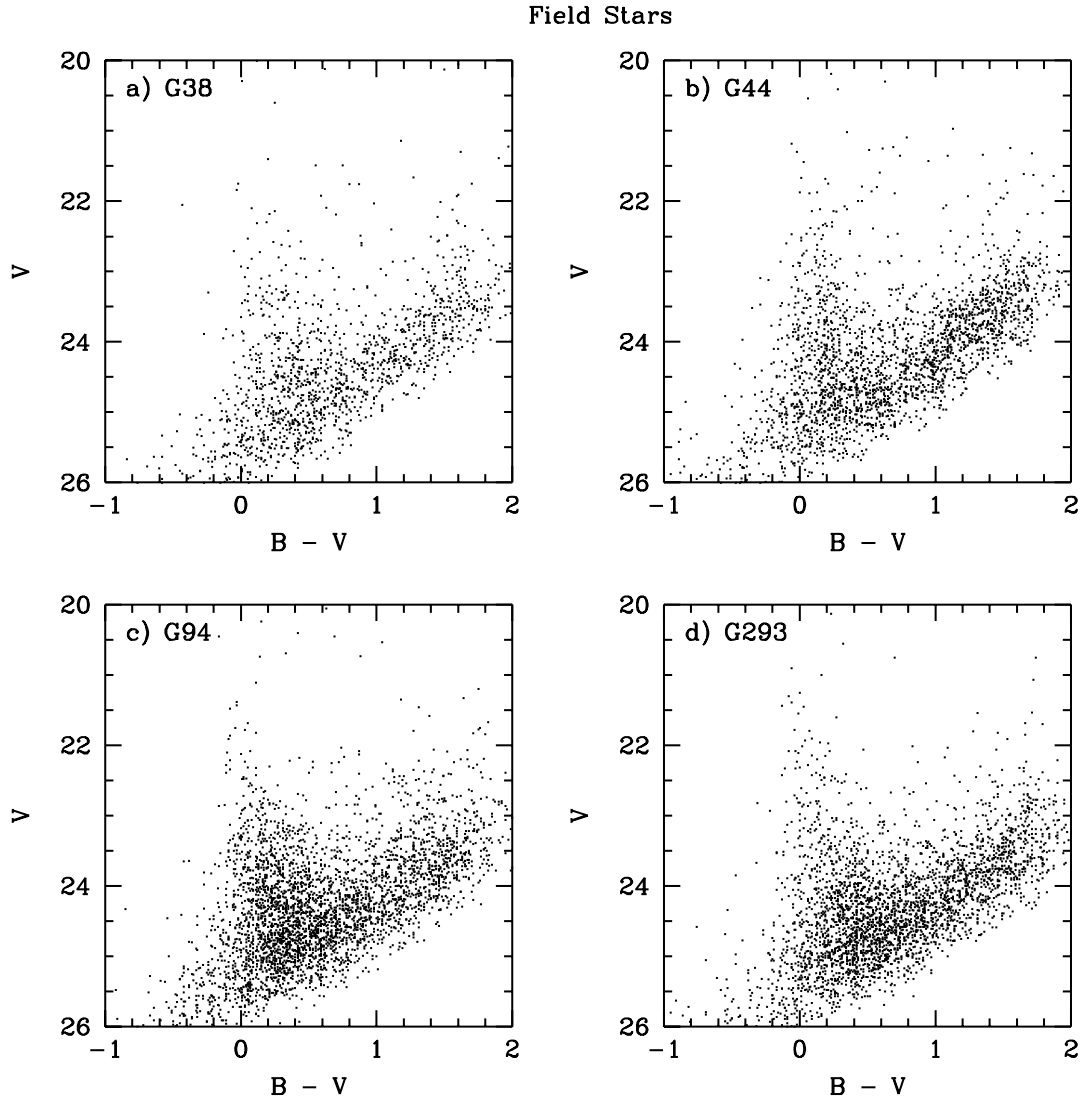


Fig. 5.— CMDs of stars at distances larger than $11.5''$ from the center of each cluster. Notice the smaller number of stars found around G38, the cluster with the largest reddening value.

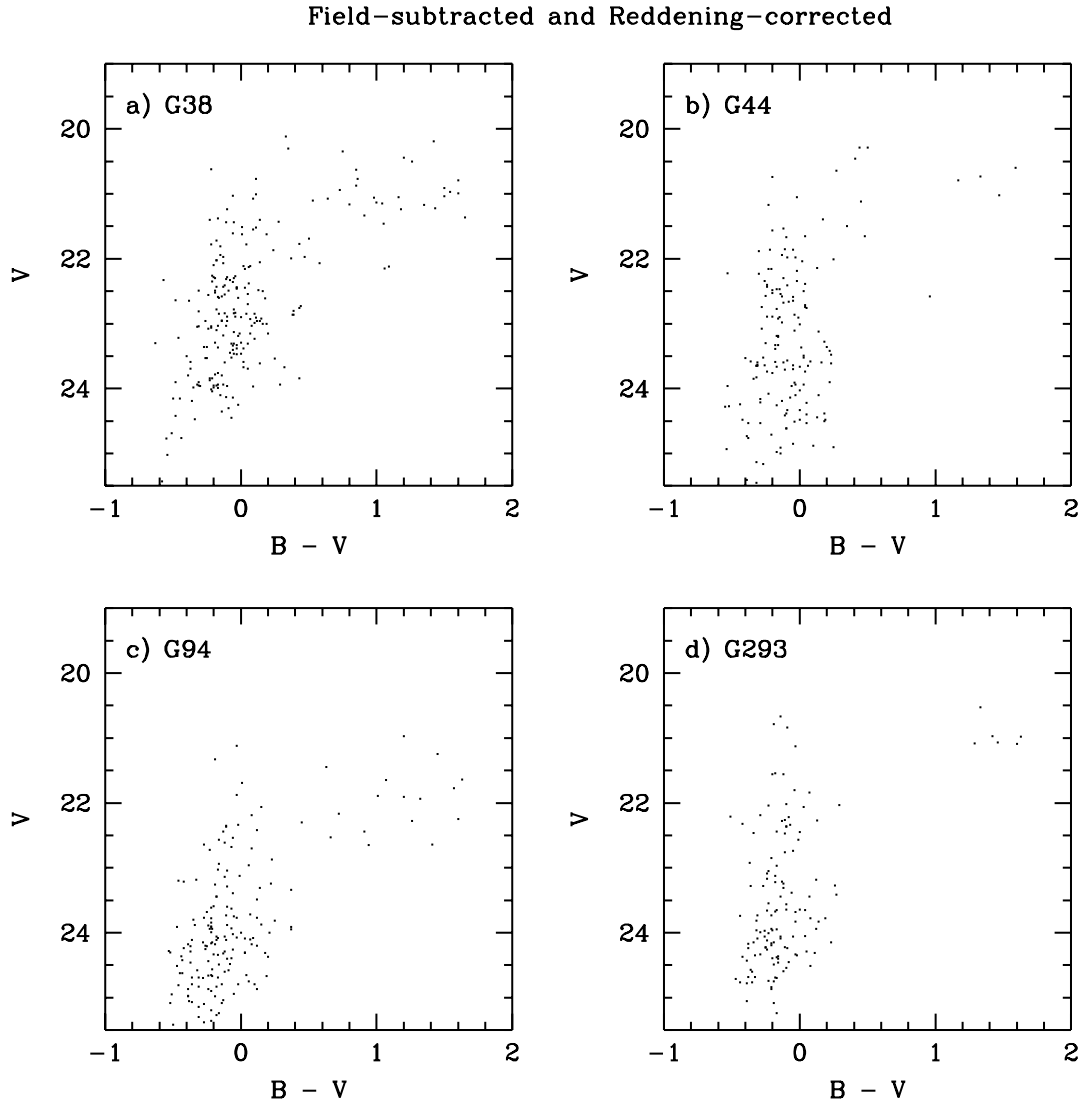


Fig. 6.— The field subtracted and reddening corrected cluster CMDs. The populous main sequence and the supergiant population were not seen in the field, and the upper main sequence was corrected to lie at the appropriate B-V color.

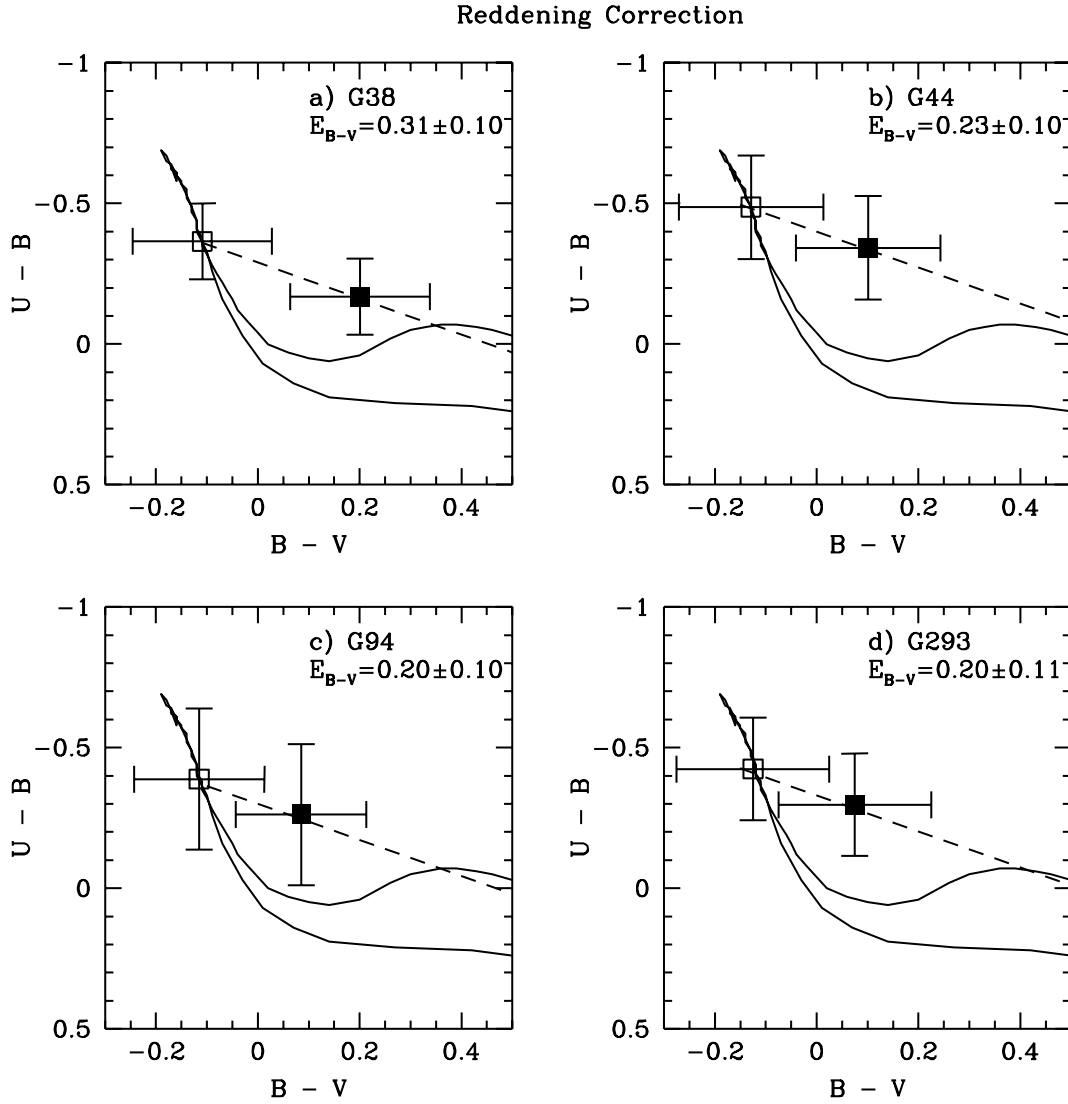


Fig. 7.— Reddening determination for the four clusters. Solid lines show the model colors for stars on the main sequence (top curve), and supergiants (bottom curve). The dotted line shows the reddening line. Closed boxes are average colors of the pre-corrected upper main sequence stars, and open boxes are the same distributions after applying our most likely reddening correction value. Our most likely reddening values and their errors are also given.

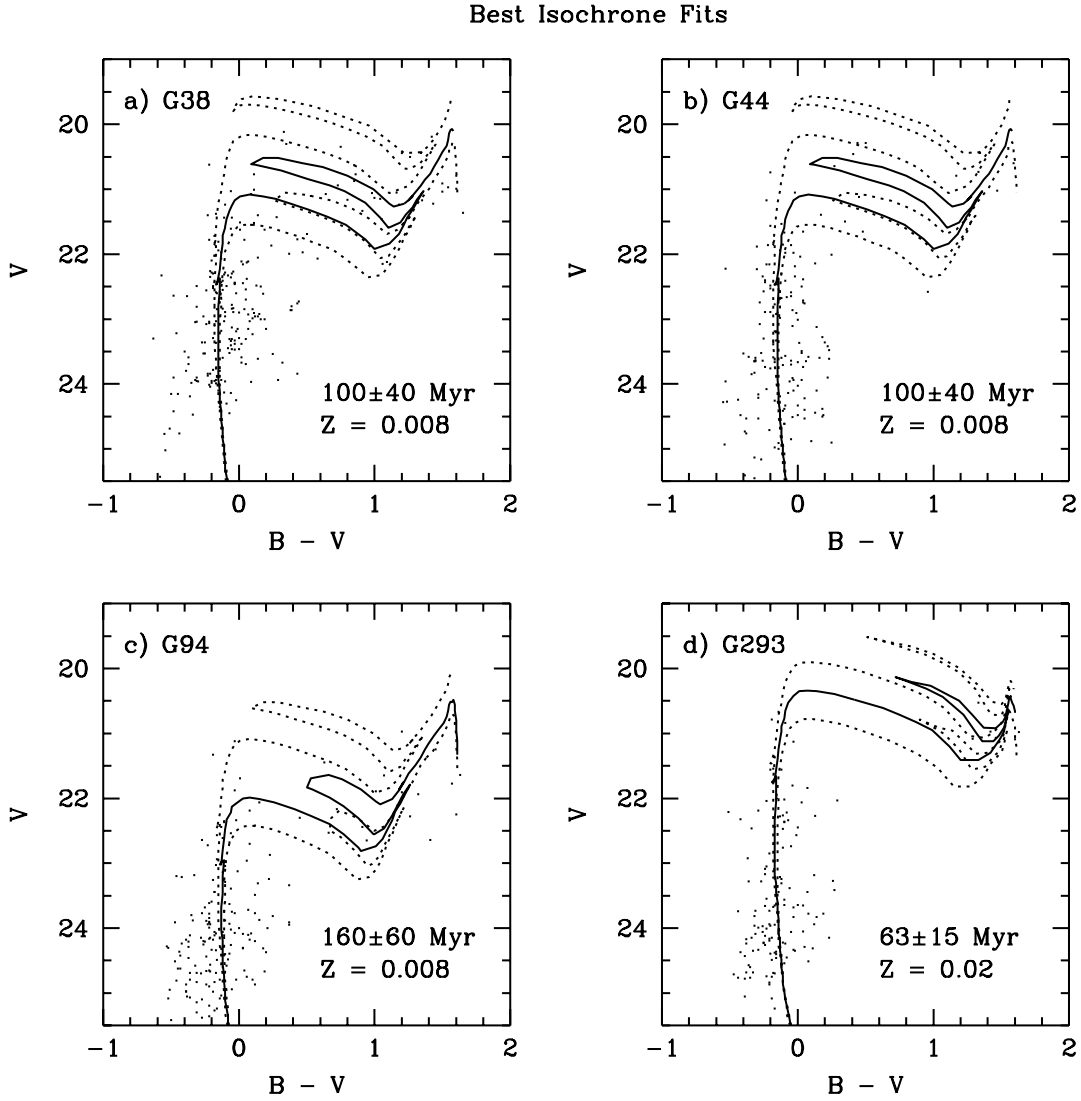


Fig. 8.— By eye age determination using model isochrones from Bertelli et al. (1994). Dotted lines mark the upper and lower limits. These were determined by finding the age where the blue loops fell below and above the location of the supergiants. The solid isochrones mark our best fits for the turnoff age. The metallicities of the isochrones were chosen based on the distribution of the supergiants, and may not be reliable.